

## Article

# Experimental Investigation on Structural Performance Enhancement of Brick Masonry Member by Internal Reinforcement

Kiwoong Jin <sup>1</sup>, Ho Choi <sup>2</sup> and Chunri Quan <sup>3,\*</sup>

<sup>1</sup> Department of Architecture, School of Science and Technology, Meiji University, Kanagawa, Kawasaki 2148517, Japan; jin@meiji.ac.jp

<sup>2</sup> Department of Architecture, Faculty of Science and Technology, Shizuoka Institute of Science and Technology, Fukuroi 4378555, Japan; choi.ho@sist.ac.jp

<sup>3</sup> Department of Architecture, Graduate School and Faculty of Engineering, Osaka Institute of Technology, Osaka 5358585, Japan

\* Correspondence: chunri.quan@oit.ac.jp

**Abstract:** This study focused on perforated bricks, and the structural performance enhancement of brick members by internal reinforcement was experimentally investigated. As a new reinforcing material, screw iron (SI) rods were selected for the internal reinforcement, and they were inserted into the perforated brick. To investigate the most-effective reinforcing method as well as to understand the fundamental structural behaviors, four specimens with different variables were fabricated, and three-point bending tests were carried out. From the experiments, it was found that the maximum strength of the specimen increased by more than two times with internal reinforcement. The internal reinforcement, fixed by nuts at both ends of the specimen to enhance integrity, increased the maximum strength by nine times. Moreover, the deformation capacities of the specimens were also greatly enhanced. The case where the internal SI rods were fixed by nuts without mortar also showed a similar structural performance to the case with mortar. The estimation methods of the maximum strength of the specimens were also discussed, and they showed reasonable agreement with the test results. It was proved that the proposed material and methods enabled effective utilization of the internal reinforcement, and they could contribute to the improvement of structural performances in masonry construction.

**Keywords:** reinforced masonry structure; stilt house; perforated brick; internal reinforcement; screw iron rod; bonding action; fixing of reinforcement; mortar filling work



**Citation:** Jin, K.; Choi, H.; Quan, C. Experimental Investigation on Structural Performance Enhancement of Brick Masonry Member by Internal Reinforcement. *Appl. Sci.* **2023**, *13*, 5287. <https://doi.org/10.3390/app13095287>

Academic Editor: José Neves

Received: 4 April 2023  
Revised: 19 April 2023  
Accepted: 21 April 2023  
Published: 23 April 2023



**Copyright:** © 2023 by the authors. Licensee MDPI, Basel, Switzerland. This article is an open access article distributed under the terms and conditions of the Creative Commons Attribution (CC BY) license (<https://creativecommons.org/licenses/by/4.0/>).

## 1. Introduction

There are many residential buildings with raised floors, called stilt houses, in the region of South East Asia to protect human lives and properties from floods caused by frequent heavy rain. In particular, for private houses, superstructures constructed on raised floors are very common, where the floors are supported by stilts, as shown in Figure 1. For the reasons of construction cost and workability, the stilt sometimes consists of plain concrete with no reinforcement or wood materials. However, such plain concrete stilts are likely to be vulnerable to horizontal forces such as wind loads, seismic loads, and tsunamis. Wood stilts are less expensive than plain concrete and are economical. Nevertheless, their structural performance against horizontal forces may be insufficient; furthermore, there is a risk of rot and pest damage after floods or tsunamis, and the further deterioration of their structural performances is expected (See Figure 2). On the other hand, bricks or concrete blocks (CB) are often used as building materials in this area for economic and climate reasons, and perforated bricks are among them, as shown in Figure 3. Considering the widely used tendency toward perforated bricks, it will be possible to construct a stronger

stilt by utilizing brick masonry with proper reinforcement. For instance, penetrating the perforated bricks with reinforcing bars and placing the brick stilt appropriately between the ground and the floor is one of the promising alternatives.



**Figure 1.** Stilt house in the region of South East Asia.



**Figure 2.** Tsunami damage by Sumatran Earthquake (2004).



**Figure 3.** Perforated brick.

Masonry buildings made of bricks or CB are used all over the world, and the majority of the world's population lives in properties made with this structural system. Since the 20th century, more than half of the victims of earthquakes have been caused by the collapse of masonry buildings [1]. In earthquake-prone regions around the world, there are many unreinforced masonry (URM) buildings or RC structures with URM infills. However, this structural system contains URM members; thus, their structural performances, as well as their seismic capacities, are likely to be insufficient, which would lead to serious earthquake damage, as shown in Figure 4. Therefore, a number of studies concerning the structural characteristics of URM members have been carried out, and many of them focus on URM infills. For URM infills, their diagonal strut mechanism and the interaction between their boundary frames and infills are focused on in the previous studies [2–9]. In addition, their in-plane seismic behaviors against lateral loads, having different types of URM units and boundary frames, were investigated, based on experimental and analytical studies [10–16], and backbone curves with URM infills were proposed by some structural guidelines and researchers [17–21]. As URM structures tend to be more vulnerable to out-of-plane excitations, seismic performances against out-of-plane vibrations were also investigated by previous studies [22–24].



**Figure 4.** Brick masonry damage from Central Java Earthquake (2006).

In order to improve the seismic capacity of URM structures, reinforcing or retrofitting methods were developed, and the seismic performances of reinforced masonry (RM) members against in-plane and out-of-plane loadings were evaluated by previous studies [25–48]. Some of them used new materials with steel fiber or waste marble powder [25,26]. Many of them employed outer-surface reinforcing or retrofitting schemes by using ferrocement, reinforced plaster, shotcrete, fiber-reinforced polymers [27–34], etc. In a few cases, reinforcing methods by internal steel reinforcement were conducted for masonry members [35–38]. They were usually for the CB units with relatively large holes, and some focused on the reinforcement of the bed joint mortar. Prestressing techniques by post-tensioning forces were also applied to the masonry members [35–46], and some reinforcing schemes were introduced in the design codes and guidelines [47,48]. The prestressing forces were provided by external or internal tendons such as high-strength strands and steel bars. On the other hand, such post-tensioning skill is somewhat difficult to apply to small structures and increases the construction cost. Measuring or managing the tension stress of tendons would also be complicated.

Especially for the brick member, it has been common practice to apply reinforcing materials to the outer surface, and there were few attempts focused on internal reinforcing. Moreover, the structural performances of out-of-plane behaviors were less considered. Hence, in the previous study by the authors of [49], the deformed reinforcing bars were arranged inside the perforated bricks, supposing the brick stilt member mentioned earlier, and their structural performances, in the out-of-plane direction, were experimentally investigated. Although the enhancement in structural performance was obtained to some extent, it was found that the reinforcing effect could be drastically decreased when the bond action and integrity between the internal bars and mortar was poor, which was indicated as an important future task. Therefore, in this study, a crucial improvement was made to enhance those defects between internal reinforcement and mortar by using new reinforcing materials and methods, and its effectiveness was verified based on experimental discussions, which could provide more robust stilts and brick members.

## 2. Experimental Program

### 2.1. Material Properties

Figure 5 shows an overview of the materials selected in this study. As shown in the Figure, a screw iron (SI) rod was employed as a new reinforcing material. Perforated bricks with three holes, produced in Japan, were employed in this study since the local products of the region of South East Asia were not available. It was noted that the main purpose of this study was the application of SI rods to perforated bricks and the investigation of the internal reinforcing effects on structural performance; therefore, the perforated bricks from Japan were adopted at this time. The mortar mix proportion of sand, cement, and water was 11:1:1 (weight ratio). In addition, in order to solve the problem of the integrity and bonding behaviors between the steel bars and mortar, which were raised in the previous study by the author [49], the use of deformed reinforcing bars with screws (threaded reinforcing bars) was first considered. By fixing the bricks at both ends using screw reinforcing bars and nuts, it was thought that the integrity of the members as well as the bonding between the reinforcing bars and mortar could be assured. On the other hand, SI rods, which were

easily available compared to screw reinforcing bars, were selected as a new reinforcing material. Hence, M14 with a nominal cross-sectional area of  $115 \text{ mm}^2$  was used for the SI rods, and the steel plate was attached to both ends of the brick member in some specimens, as explained later. It was noted that the thickness of the steel plate (9 mm) was selected after examining the bearing pressure of the nut and the safety against the punching shear.

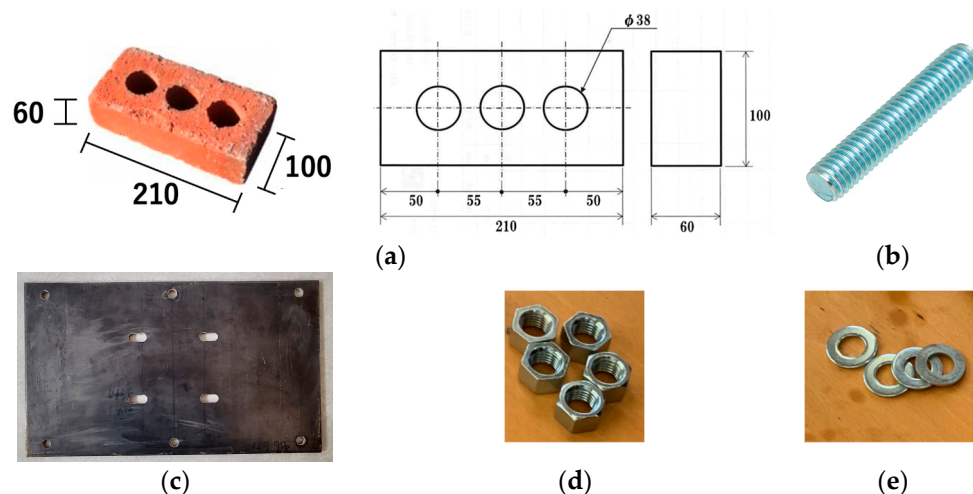


**Figure 5.** Selected material in this study: (a) Perforated brick (mm); (b) Screw iron rod (M14); (c) Steel end plate; (d) Nut; (e) Washer.

Tables 1–3 show the material test results, and the values are the mean values of 3 samples in each test. For the material tests, a compression test of the brick unit and the 3-layer stacked prism, a push-out test of the 3-layer stacked prism, mortar compression and splitting tests, and a tensile test of the SI rod were carried out. Herein, two types of 3-layer stacked prisms were fabricated, which were the cases with or without the SI rods. A total of three SI rods were inserted into each hole. The compressive strength of the 3-layer stacked prism was 21.1 MPa in the case without SI rods and 23.0 MPa in the case with SI rods. From this result, the effect of the reinforcing rod on the compressive strength was regarded to be slight. On the other hand, from the push-out test, the shear strength was found to be 0.7 MPa when the stacked prism had no SI rods, and the shear strength with SI rods was calculated to be 3.2 MPa. Through these material test results, it was confirmed that the iron rods did not contribute much to the increase in compressive strength but had great effects on the shear strength. The 0.2% offset method was used to determine the yield point of the SI rod because there was no clear yield point from the tensile test.

**Table 1.** Material characteristics of brick unit and mortar.

|                             | Brick Unit | Mortar   |
|-----------------------------|------------|----------|
| Compressive strength        | 39.1 MPa   | 15.1 MPa |
| Tensile strength $\sigma_T$ | —          | 0.9 MPa  |

**Table 2.** Material characteristics of brick prism (3-layer stacked).

|                                 | Brick Prism without SI Rod | Brick Prism with SI Rod |
|---------------------------------|----------------------------|-------------------------|
| Compressive strength            | 21.1 MPa                   | 23.0 MPa                |
| Shear strength by push-out test | 0.7 MPa                    | 3.2 MPa                 |

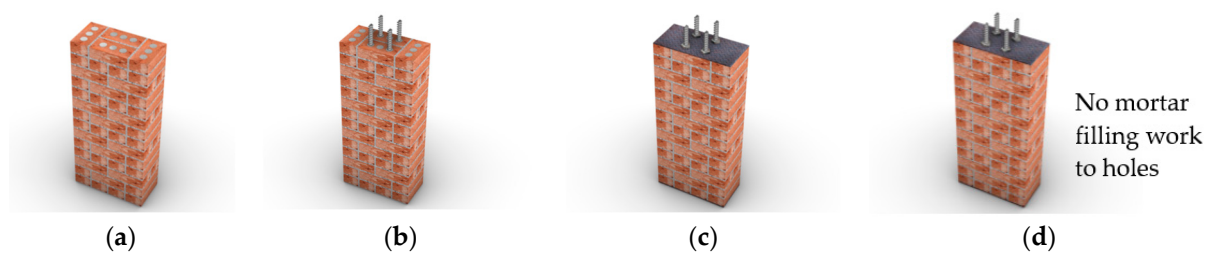
**Table 3.** Material characteristics of screw iron (SI) rod.

| Yield Strength $\sigma_y$ (MPa) <sup>*a</sup> | Yield Strain $\varepsilon_y$ ( $\mu$ ) <sup>*a</sup> | Tensile Strength $\sigma_t$ (MPa) |
|---|--|-----------------------------------|
| 446.9 MPa                                     | 3833 $\mu$   | 537.4 MPa                         |

<sup>\*a</sup> Strength and strains by 0.2% offset method.

## 2.2. Specimen and Experiment Outline

Figure 6 shows a conceptual diagram of the test specimens. Four specimens were fabricated in total. First, the UBM (Unreinforced Brick Member) specimen consisted of perforated bricks and mortar without any reinforcement, and, in the IRBM (Internally Reinforced Brick Member) specimen, an internal reinforcement of four SI rods was added. From these two specimens, the internal reinforcing effect of the SI rods was examined. Next, in the IRBM—F (Internally Reinforced Brick Member Fixed by nut) specimen, the four SI rods were fixed by nuts after sandwiching both ends of the specimen with steel plates to enhance integrity. As mentioned earlier, according to the previous test results [49], the flexural strength of the specimen increased when the bonding performance between the steel and mortar was sufficiently secured. Therefore, in order to enhance structural performance, fixing work with steel plates and nuts was introduced. It was noted that every hole of the perforated brick was filled with mortar in IRBM—F. On the other hand, the mortar filling work to the holes was omitted in the IRBM—FNM (Internally Reinforced Brick Member Fixed by nuts with No filling Mortar) specimen to further improve workability as well as to save on costs and materials. The internal SI rods were fixed by nuts at both ends of the specimen, and the joint mortar was only employed on each layer between bricks in the IRBM—FNM.

**Figure 6.** Conceptual diagram of test specimens: (a) UBM; (b) IRBM; (c) IRBM—F; (d) IRBM—FNM.

The specimen dimensions were 210 × 430 × 970 mm (depth × width × height), and the cross-sectional details are shown in Figure 7. As was performed in the previous experiment [49], the 3 arrangement patterns shown in Figure 7 were stacked in order for 14 layers to fabricate each specimen since such a combination arrangement was thought to provide more robust resistance against lateral loading. In order to find out the effective reinforcing method as well as to understand fundamental structural behaviors, 3-point bending tests were carried out, where the distance between two supports was set to be 770 mm, as can be seen in Figures 7 and 8. In the 3-point bending test, the vertical deflection of the specimen was measured at three points by displacement transducers (LVDTs). The strains at the crucial points of the SI rods were also measured for the specimens with internal reinforcements. It was noted that B1~B3 and T1~T3 represented the strains of the bottom and top side rods, respectively. From those strains, bond stresses between the mortars and rods were calculated to investigate the bonding performance, as discussed later in Section 3. All the specimens were fabricated by non-experts such as lab students, supposing self-buildable economic housing. In the specimens with SI rods, the rods were fixed vertically in advance, and then the masonry work was carried out by passing the perforated bricks through the rods. The bricks were stacked one-by-one, and mortar works were applied at the same time. The accuracy of the mortar filling work was likely to vary depending on the workers. Hence, it may have affected the bonding performance between the mortars and SI rods, which was the reason why the rods were fixed by steel plates and

nuts in IRBM—F and IRBM—FNM. It was also noted that the ends of the SI rods were lightly tightened with nuts using human power after curing the mortar; thus, the initial prestressing force was little.

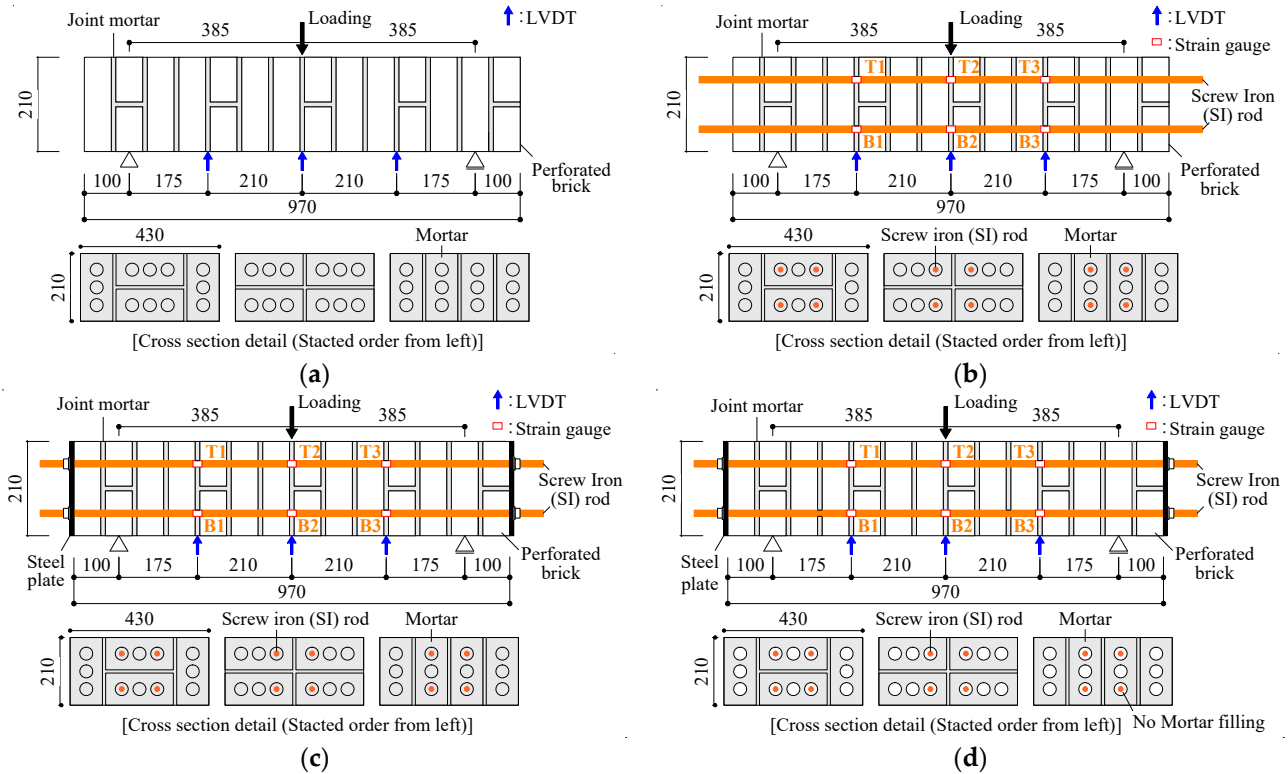


Figure 7. Specimen and experiment details: (a) UBM; (b) IRBM; (c) IRBM—F; (d) IRBM—FNM (mm).



Figure 8. 3-point bending test in this study: (a) Example of IRBM; (b) Example of IRBM—F.

### 3. Experiment Results

#### 3.1. UBM (Unreinforced Brick Member)

Figure 9a shows the final failure pattern, and the red line represents the main crack developed in the specimen. Figure 10a shows the vertical load–deflection relationship, in which the horizontal axis represents the vertical deflection at the center of the span. In this specimen, the load increased almost linearly up to a maximum strength with the increase in the vertical deflection. However, a flexural crack developed in the joint mortar at the center of the span, and a sudden brittle failure occurred. As can be seen in Figure 10a, the maximum strength recorded in this specimen was 13.96 kN, and the vertical deflection at the maximum strength was 0.26 mm. By defining the deflection angle ( $R$ ) as the ratio of vertical deflection to the half span, the failure  $R$  was only 0.068%, which exhibited poor deformation capacity. Therefore, sufficient deformation capacity cannot be expected

without any reinforcement on the brick masonry. The calculation result of the maximum strength will be discussed in Section 4.

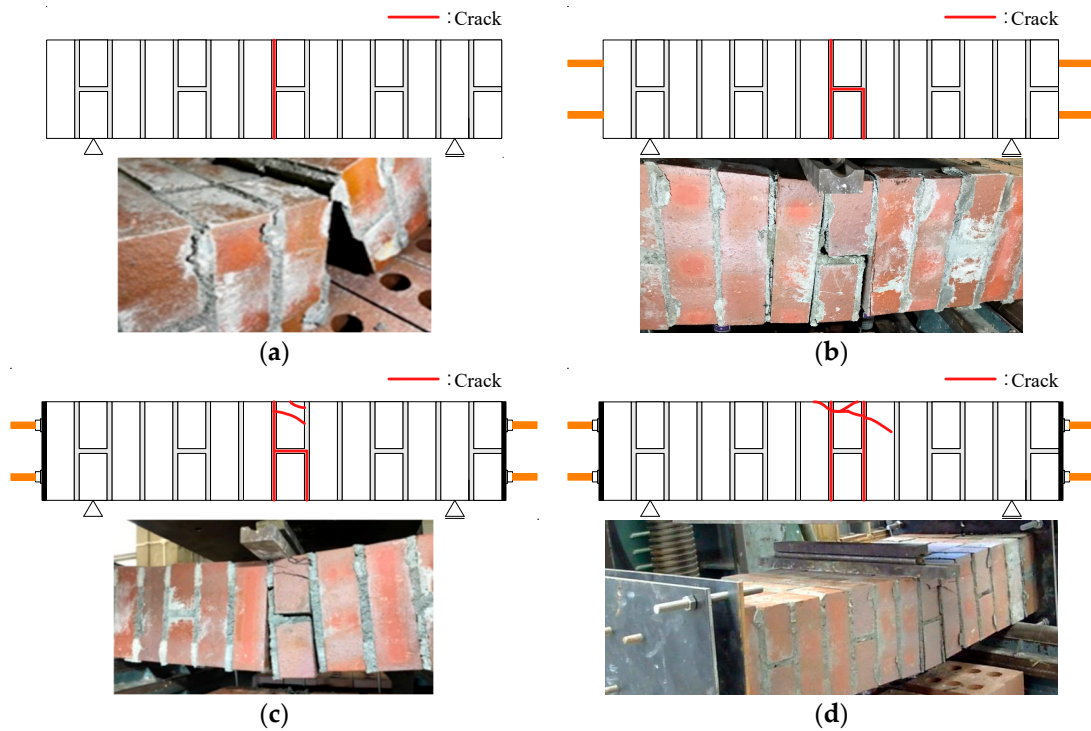


Figure 9. Crack patterns: (a) UBM; (b) IRBM; (c) IRBM—F; (d) IRBM—FNM.

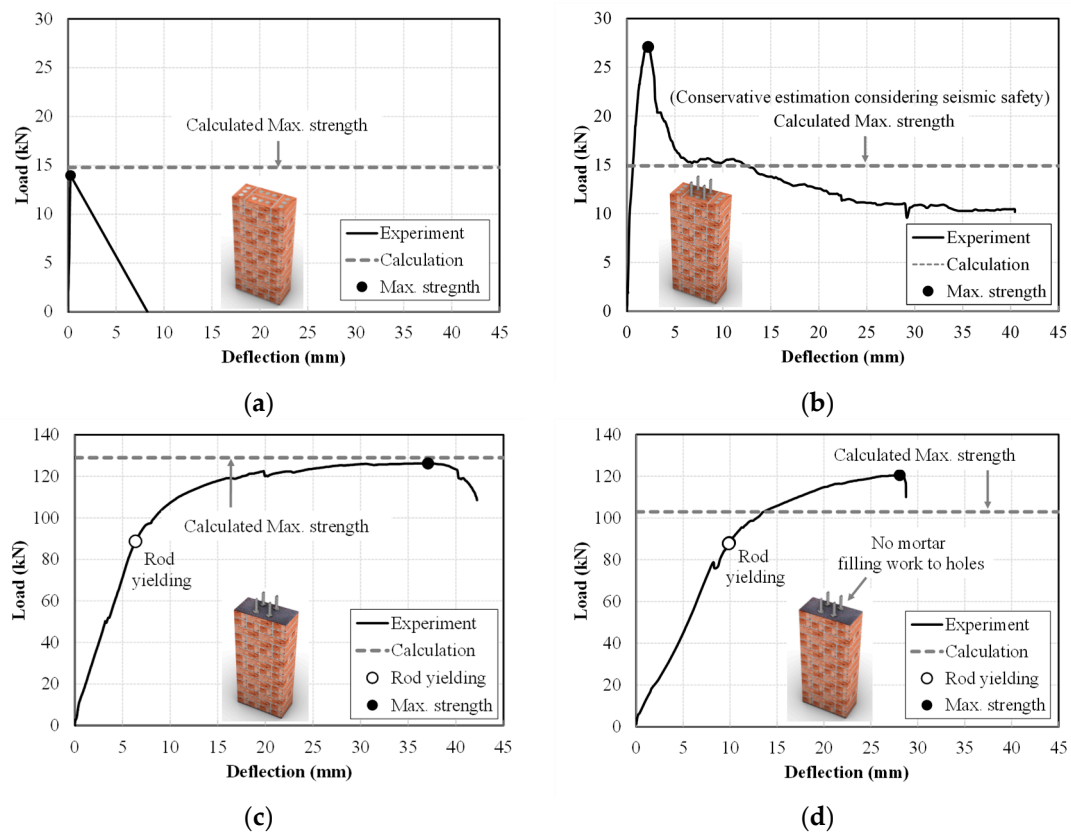
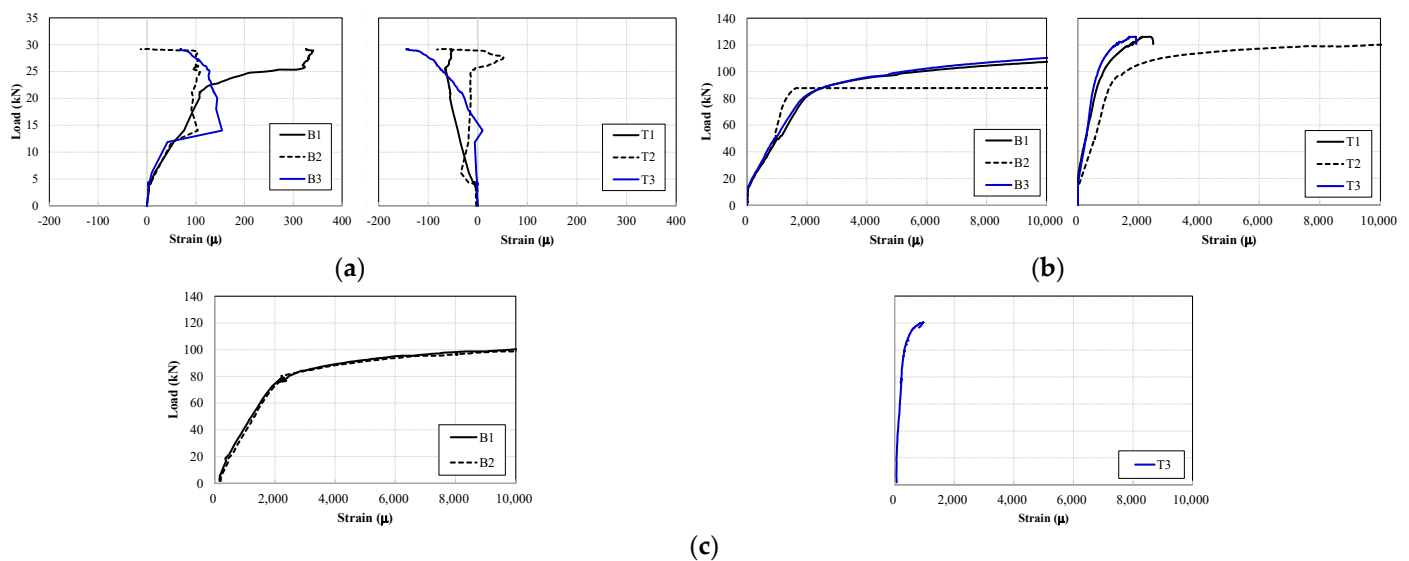


Figure 10. Load–deflection relationship: (a) UBM; (b) IRBM; (c) IRBM—F; (d) IRBM—FNM.

### 3.2. IRBM (*I*nternally *R*einforced *B*rick *M*ember)

In this specimen, the internal reinforcement by SI rods was supplemented. Figure 9b shows the final failure pattern, and Figure 10b shows the vertical load–deflection curve. As the vertical deflection grew, a flexural crack occurred near the middle of the span, but there was no sudden strength drop, such as in the UBM. Although the flexural crack occurred, the specimen maintained a continuous strength increase to some extent, and the strength reached its maximum when the flexural crack completely progressed up to the extreme compression fiber of the damaged section. A maximum strength of 27.08 kN was recorded, which was about twice that of the UBM; in addition, the vertical deflection was 2 mm, which was greater than 7 times that of the UBM. After that, a sharp strength drop initiated just after the complete crack was opened, but approximately 40% of the maximum strength was maintained until the vertical deflection of 40 mm. At this time, a slight compression failure occurred, and damage was found on the joint mortar at the extreme compression fiber, but a stable residual strength was kept due to the SI rods and their bending resistance.

Figure 11a shows the relationship between the vertical load and strains of SI rods. The strain values of the top side (T1~T3) were very small. Although those of the bottom side (B1~B3) were larger than those of the top side, the strain at the maximum strength was only about  $350\mu$ , and it was judged that the bonding condition between the rod and mortar was very poor. Comparing the extra length of the rods (See Figure 8a), which came out from the specimen before and after the test, the extra length was shortened by about 20 mm on average, which meant a slip behavior in the rods during loading.



**Figure 11.** Vertical load–strain relationship: (a) IRBM; (b) IRBM–F; (c) IRBM–FNM.

### 3.3. IRBM–F (*I*nternally *R*einforced *B*rick *M*ember *F*ixed by Nut)

In this specimen, the SI rods were fixed by nuts after sandwiching both ends of the specimen with steel plates to enhance integrity. Figures 9c and 10c show the final crack pattern and the vertical load–deflection relationship, respectively. The yielding point of the bottom side rod is plotted in Figure 10c. In this specimen, stiffness degradation was observed after flexural crack development, and a significant stiffness decrease was found near the yielding point of the rod, which was a behavior quite similar to the reinforced concrete (RC) member. After the reinforcing rod yielded, the vertical strength gradually increased, and its maximum strength was recorded when the vertical deflection reached about 37 mm. At this time, the neutral axis depth was observed to be almost located at the extreme compression fiber of the damaged section, and the compression failure of the joint mortar and bricks was very severe. As shown in Figure 10c, a maximum strength of 126.2 kN was recorded, demonstrating more than four times the maximum

strength of the IRBM specimen. It was also noted that the  $R$  at its maximum strength was about  $1/10$ , which was an extremely large deformation. There was no abrupt strength decrease after the maximum strength was obtained, but the fracture of the bottom rod occurred at the moment when the vertical deflection reached 40 mm, which resulted in sudden failure. Therefore, even though the strain of the rod at the maximum strength could not be measured, the stress at the bottom rod was considered to reach its tensile strength. Such a failure pattern, shown in this specimen, is very dangerous, but it should be emphasized that it occurred at an extremely large deformation, larger than  $R = 1/10$ . From the load–deflection curve of IFBM—F, superior structural behaviors were achieved by the proposed material and method.

The strain distribution of the bottom and top reinforcing rods is shown in Figure 11b. As can be found in the Figure, compared to IRBM, the strain values of the rods in IRBM—F show much larger values. All the strain values of the bottom rods exceeded the yielding strain, and the strain of T2 also yielded at the maximum strength. From the strain data, fixing the SI rods with steel plates and nuts enabled the efficient use of the reinforcement, and great performance enhancements were obtained in both the strength and the deformation capacities. It should be also noted that the compressive force was acting on the brick members as a reaction force to the tensile force of the rods as the deformation grew; therefore, it not only improved the integrity of the member but also led to an increase in shear and bending resistances.

#### 3.4. IRBM—FNM (*Internally Reinforced Brick Member Fixed by Nut with No Inside Mortar*)

In this specimen, the mortar filling work to the holes of the bricks was eliminated for better workability as well as cost and material savings. The joint mortar was only employed on each layer between the bricks, and the SI rods were then fixed by nuts at both ends of the specimen; therefore, the reinforcing rods were under the unbonded condition with no bonding action [50]. Figure 9d shows the final crack development, and Figure 10d shows the vertical load–deflection curve. In this specimen, a flexural crack occurred in the middle part of the span, and it caused stiffness degradation. Moreover, a clear stiffness decrease was observed near the yield point of the bottom rod. A rigid-body rotation around the extreme compression fiber occurred at the center of the span, and a maximum strength of 120.47 kN was recorded near the vertical deflection of 27 mm. The maximum strength was slightly lower than IFBM—F, but it was still more than four times that of the IRBM. Meanwhile, the mortar and bricks on the compression fibers were crushed without any rod fracture, and an abrupt strength degradation developed. It should be noted that the  $R$  at the maximum strength was about  $1/15$ , which was also an extremely large deformation. Unlike IFBM—F, there was no filling mortar inside the holes; thus, the resistance against the compression force was weaker than that of IFBM—F. It is the reason why the compression failure preceded the rod fracture in this specimen. In addition, the SI rod in this specimen was in an unbonded state with no bonding action; thus, its strain was uniformly distributed along the length, and the strain increment of the rod was delayed [50–52]. The stiffness tended to be slightly lower than IFBM—F due to the unbonded characteristics, but almost similar strength and deformation capacities were obtained.

Figure 11c shows the strain distribution of the SI rods. Some of the strain data were not measured, and only available data were plotted in the figure. The bottom rod exceeded its yield strain with the increase in vertical deflection. On the other hand, the top rod was found not to yield until the end of the loading, which was also attributed to the unbonded characteristics [50–52]. Nevertheless, compared to IRBM with no integrity by the steel plate and nuts, the strain values of the rods exhibited much higher values. Although the filling mortar inside the holes did not exist, effective use of the reinforcement and structural performance improvements could be achieved by providing the SI rods with adequate fixing conditions. As mentioned earlier, the compressive forces, which are a reaction force to the tensile force of the rods, increased as the deformations grew; thus, the integrity of the member as well as the shear and bending capacities were enhanced.

## 4. Discussion

### 4.1. Bond Stress between Mortar and Reinforcing Rod

For IRBM and IRBM—F, where the bonding action between the filling mortar and rods was working, the bond stress ( $\tau_s$ ) was calculated by Equation (1) [53], and its maximum value ( $\tau_{s,max}$ ) was investigated. It was noted that  $\tau_s$  was calculated until the loading step, where the strain data could be reliable.

$$\tau_s = (A_r \cdot \sigma - A_r \cdot \sigma') / (\pi \cdot d_r \cdot l) = (\sigma - \sigma') \cdot d_r / (4 \cdot l) \quad (\text{MPa}) \quad (1)$$

where  $A_r$  is the cross-sectional area of the SI rod,  $\sigma$  and  $\sigma'$  are the stress of adjacent SI rods,  $d_r$  is the rod diameter, and  $l$  is the distance between adjacent SI rods.

In the IRBM, the  $\tau_{s,max}$  between the rod and mortar was calculated to be in the range of 0.18~0.85 MPa, which were quite small values. From this result and the strain distribution of the rod, the deterioration of the bonding performance was initiated from the early stage of the loading, and the result was found similar to that of the previous study [49]. In order to understand the relationship between  $\tau_{s,max}$  and the bond splitting strength ( $Kf_b$ ),  $Kf_b$  was calculated by Equation (2), according to the AIJ's guidelines [54]. It should be noted that the value calculated by the AIJ standard represented the bond strength between the concrete and longitudinal reinforcing bars and was actually different from that of this study. However, as a reference value, the evaluation of the bond strength between mortar and SI rods was attempted using the RC standard. As a result,  $Kf_b$  was calculated to be 2.43 MPa, far overestimating the experimental results. Nevertheless, considering that the maximum strength of the UBM specimen was 13.96 kN, the presence or absence of the SI rods greatly affected the maximum strength. In addition, even after the strength degradation, the IRBM maintained an almost constant residual strength up to an extremely large deformation. However, the UBM exhibited an abrupt brittle failure immediately after its maximum strength.

$$Kf_b = \left( 0.3 \left( \frac{C + W}{d_r} \right) + 0.4 \right) (F_c / 40 + 0.9), \text{ where } 0.3 \left( \frac{C + W}{d_r} \right) + 0.4 \leq 2.5 \text{ MPa} \quad (2)$$

where  $C$  is the minimum value between  $3d_c$  ( $d_c$ : smallest cover concrete depth) and longitudinal reinforcement spacing,  $W$  is the index exhibiting the effect of shear reinforcement, and  $F_c$  is the concrete compressive strength. In Equation (2), the value of  $C$  should be less than  $5d_r$ , and  $W$  becomes zero because there is no shear reinforcement.

In IRBM—F,  $\tau_{s,max}$  was estimated as 1.39~2.91 MPa, and the bond degradation was observed after those maximum values. Essentially, the calculation result of  $Kf_b$  was the same as IRBM. As a result, the  $Kf_b$  was 2.43 MPa, and the  $\tau_{s,max}$  in this specimen generally corresponded to  $Kf_b$ . It was noted that  $Kf_b$  was a reference value, but it was verified by providing the brick members with better integrities and fixing conditions, and the bonding performances were also improved.

### 4.2. Maximum Strength Evaluation

#### 4.2.1. UBM (Unreinforced Brick Member)

As explained earlier, the vertical force increased linearly up to the maximum strength as the vertical deflection increased. After a flexural crack developed in the joint mortar at the middle of the span, sudden brittle failure occurred when recording the maximum strength. Therefore, in this study, the maximum strength  $Q_{max,UBM}$  was evaluated from Equations (3) and (4) by elastic theory, where  $M_{cr}$  was the cracking moment. The calculated  $Q_{max,UBM}$  was 14.84 kN and was plotted along with the test results in Figure 10a. The estimation result was also compared with the experiment's results in Table 4. As can be seen in the Figure and Table, the ratio from the calculation to the experiment of the maximum strength was 1.06, and they showed good agreement.

$$M_{cr} = \sigma_T Z \quad (3)$$

$$Q_{max,UBM(IRBM)} = \frac{4M_{cr}}{l} \quad (4)$$

where  $\sigma_T$  is the mortar tensile strength by splitting test shown in Table 1 (0.9 MPa in this study),  $Z$  is the section modulus, and  $l$  is the distance between both supports shown in Figure 7 (770 mm in this study).

**Table 4.** Maximum strength calculation results.

| Specimen | $Q_{max,cal}$ (kN)  | $Q_{max,exp}$ (kN) | $Q_{max,cal}/Q_{max,exp}$ |
|----------|---------------------|--------------------|---------------------------|
| UBM      | 14.84               | 13.96              | 1.06                      |
| IRBM     | 14.84 <sup>*a</sup> | 27.08              | 0.55                      |
| IRBM—F   | 129.43              | 126.20             | 1.03                      |
| IRBM—FNM | 102.92              | 120.47             | 0.85                      |

<sup>\*a</sup> Conservative estimation considering seismic safety.

#### 4.2.2. IRBM (Internally Reinforced Brick Member)

As this specimen has internal reinforcement, the maximum strength was higher than that of UBM. Therefore, at first, the maximum strength evaluation was attempted by applying Equation (5), which was the flexural moment ( $M_y$ ) formula of a RC beam member, as per the AIJ guidelines [54]. However, the calculation result was 2.8 times the test result and highly overestimated the experiment. This was because the bonding conditions between the SI rod and filling mortar were very poor and completely deteriorated before the maximum strength. Thus, the strain increment of the rod was also little, and the expected flexural strengths like RC members could not be exhibited. In this way, when reinforcing only by SI rods without any fixing work, the bonding performance could not be guaranteed, and it was difficult to specify the strain and stress of the SI rods at the maximum strength point. Therefore, considering the seismic safety and conservative performance evaluations, the maximum strength  $Q_{max,IRBM}$  was estimated by the cracking strength of Equations (3) and (4), which was the same as UBM.

$$M_y = 0.9a_t\sigma_y d \quad (5)$$

where  $a_t$  is the cross-sectional area of longitudinal reinforcement (230 mm<sup>2</sup> in this study),  $\sigma_y$  is the yield strength of longitudinal reinforcement (446.9 MPa in this study), and  $d$  is the effective depth defined as the distance between extreme compression fiber and reinforcement at the tensile side (160 mm in this study).

#### 4.2.3. IRBM—F (Internally Reinforced Brick Member Fixed by Nut)

In this specimen, from the strain data above, effective use of the reinforcement was confirmed by fixing the SI rods, which resulted in a great improvement in structural performance. As a result, the stress of the bottom rod was expected to reach its tensile strength at the maximum strength point, and that of the top rod was found to exceed its yield strength. Therefore, for the maximum strength evaluation, the stresses of the bottom and top rods were set to be the tensile ( $\sigma_t$ ) and yield ( $\sigma_y$ ) strengths, respectively, which were obtained from the material test (See Table 3). It was also noted that when the maximum strength was recorded, the neutral axis depth was very short, and the neutral axis was quite close to the extreme compression fiber of the damaged section since the cross-section had a relatively wide width (430 mm) compared to the depth (210 mm). Therefore, for simplicity, the neutral axis was assumed to be located at the extreme compression fiber, and the force equilibrium condition at the damaged cross-section was set to be as in Figure 12. The maximum strength  $Q_{max,IRBM-F}$  was then evaluated from Equations (6) and (7), where  $\sigma_t$  and  $\sigma_y$  in Table 3 were substituted for the bottom rod stress ( $\sigma_{br}$ ) and the top rod stress ( $\sigma_{tr}$ ), respectively. The calculated  $Q_{max,IRBM-F}$  was 129.43 kN and was shown together with

the test results in Figure 10c. The estimation value was also compared with the experiment value in Table 4. As can be seen in the Figure and Table, the ratio of the calculation to the experiment of the maximum strength was 1.03, and the evaluation result exhibited good accuracy.

$$M_{max} = A_{br} \times \sigma_{br} \times d_{br} + A_{tr} \times \sigma_{tr} \times d_{tr} \tag{6}$$

$$Q_{max,IRBM-F(IRBM-FNM)} = \frac{4M_{max}}{l} \tag{7}$$

where  $A_{br}$  is the total cross-sectional area of the bottom rod (230 mm<sup>2</sup> in this study),  $A_{tr}$  is the total cross-sectional area of the top rod (230 mm<sup>2</sup> in this study),  $\sigma_{br}$  is the stress of the bottom rod,  $\sigma_{tr}$  is the stress of the top rod,  $d_{br}$  is the distance between the extreme compression fiber and the rod position on the bottom side (160 mm in this study), and  $d_{tr}$  is the distance between the extreme compression fiber and the rod position on the top side (50 mm in this study).

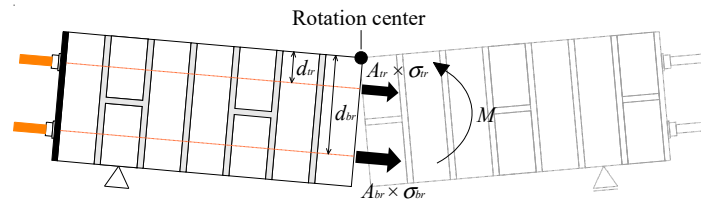


Figure 12. Force equilibrium condition.

#### 4.2.4. IRBM—FNM (Internally Reinforced Brick Member Fixed by Nut with No Filling Mortar)

In this specimen, not only could superior workability be achieved but also a remarkable enhancement in structural performance, by eliminating the mortar filling work and the fixing of the SI rods. Due to the unbonded characteristics, the strain increment was delayed compared to that of IRBM—F. Hence, from the strain data, the stress of the bottom side rod was considered to be in the range between the yield ( $\sigma_y$ ) and tensile ( $\sigma_t$ ) strength. The strain of the top side was found to be less than the yield strain ( $\epsilon_y$ ). In addition, due to no mortar filling work, the specimen tended to rotate as a rigid body, with respect to the damaged section, after the crack development at the joint mortar. The neutral axis was very close to the extreme compression fiber at the maximum strength, as was found in IRBM—F. Based on these results, as well as considering a conservative estimation of the maximum strength  $Q_{max,IRBM-FNM}$ , the strain of the bottom rod was assumed to be  $\epsilon_y$ . Then, the deformation compatibility condition was established, as shown in Figure 13. Since the SI rod was unbonded, the total elongation of the bottom rod ( $\delta_{br}$ ) could be expressed as Equation (8). When the rotation center was located at the extreme compression fiber, the relationship between  $\delta_{br}$  and the total elongation of the top rod ( $\delta_{tr}$ ) could be derived from Equation (9). The strain of the top rod ( $\epsilon_{tr}$ ) and thus its stress ( $\sigma_{tr}$ ) could be obtained based on the material test of the SI rod. Then,  $Q_{max,IRBM-FNM}$  could be calculated from Equations (6) and (7), where  $\sigma_y$  and  $\sigma_{tr}$  are substituted for the bottom rod stress ( $\sigma_{br}$ ) and the top rod stress ( $\sigma_{tr}$ ), respectively, and the estimated  $Q_{max,IRBM-FNM}$  was 102.92 kN. The evaluated value is shown along with the test result in Figure 10d and Table 4, where the ratio of the calculation to the experiment was 0.85. Even though the estimation was slightly lower than the experiment, it showed reasonable agreement with the test result.

$$\delta_{br} = \epsilon_y \times L \tag{8}$$

$$\delta_{br} : \delta_{tr} = d_{br} : d_{tr} = \epsilon_y \times L : \epsilon_{tr} \times L \tag{9}$$

where  $L$  is the total length of the rod inside the specimen (970 mm in this study).

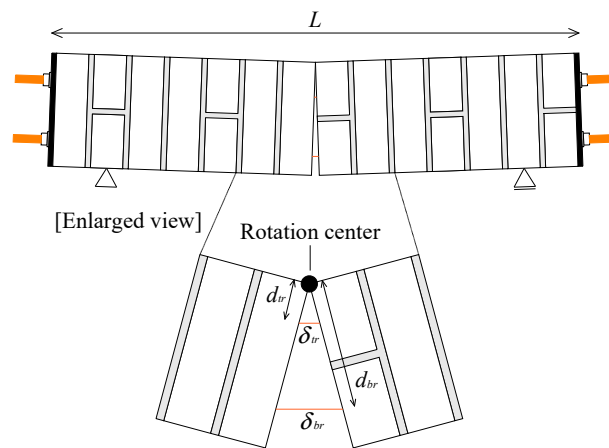


**Figure 13.** Deformation compatibility condition of IRBM—FNM with unbonded rod.

From the test results of IRBM—F and IRBM—FNM, it was proved that the proposed material and methods enabled effective utilization of the internal reinforcement, and they could contribute to the improvement of structural performance in masonry construction. On the other hand, in the test specimen, the stress of the SI rods was determined based on the experimental results. In actual cases, it is difficult to specify those stresses. Therefore, for practical use, it might be an alternative to temporarily set  $\sigma_{br}$  to be either  $\sigma_y$  or  $\sigma_t$  and  $\sigma_{tr}$  to be 0. The calculation results using these values were approximately 70~80% of the maximum strength by the experiments. Although the calculations underestimated the test results, conservative performance evaluations considering seismic safety could be achieved by these assumptions and manner.

## 5. Conclusions

In this study, effective reinforcing methods for brick masonry members were experimentally investigated, focusing on perforated bricks and a new internal reinforcing material. The following findings were the major findings obtained from this study.

1. In UBM without any reinforcement, an abrupt strength decrease occurred right after a flexural crack development, showing a load–deflection relationship with a poor deformation capacity. The failure deflection angle was only 0.068%.
2. In IRBM with SI rods, complete bonding deterioration occurred before the maximum strength and expected reinforcing effect could not be obtained. However, the maximum strength was two times that of UBM, and a stable residual strength could be maintained even after the maximum strength declined due to the bending resistances of the rods. SI rods not only increased the maximum strength but also provided better deformation capacities.
3. In IRBM—F, the SI rods fixed by steel plates and nuts provided robust integrities with the brick members and greatly enhanced the structural performance. The maximum strength was demonstrated by more than nine times that of UBM and by more than four times that of IRBM. Moreover, the strength degradation did not occur by an extremely large deformation angle of 1/10. The SI rods were efficiently utilized, and the effectiveness of the proposed material and method was verified.
4. In IRBM—FNM, the mortar filling work was eliminated for better workability as well as cost and material savings. Even in this case, the load–deflection curve was found to be almost the same as IRBM—F. Although sudden strength degradations occurred after the maximum strength, they were found at the large deformation angle of 1/15, and efficient use of the internal reinforcements was also achieved.
5. A maximum strength evaluation was carried out, and the calculation results reasonably agreed with the experimental values. The ratios of the calculations to the experiments of maximum strength were between 0.85 and 1.03 in UBM, IRBM—F, and

IRBM—FNM. The ratio was somewhat small in IRBM, but conservative estimation could be performed considering seismic safety.

The main purpose of this study was to find out and examine effective reinforcing methods by a new material. Hence, various experimental variables were focused on, rather than the number of specimens, and three-point bending tests were carried out. From the experiments, by fixing the SI rods via steel plates and nuts, the structural stabilities of the brick masonries were enhanced, and the process's effectiveness was successfully verified. For future research, more verification by using a large number of specimens will be also required for practical uses, and it is necessary to investigate, in detail, the seismic behavior when receiving an inverse symmetrical moment assuming an actual lateral load.

**Author Contributions:** Conceptualization, K.J.; Investigation, K.J., H.C. and C.Q.; Resources, K.J.; Data curation, K.J., H.C. and C.Q.; Writing—review & editing, K.J., H.C. and C.Q.; Visualization, K.J.; Supervision, K.J., H.C. and C.Q.; Funding acquisition, K.J. All authors have read and agreed to the published version of the manuscript.

**Funding:** This research received no external funding.

**Institutional Review Board Statement:** Not applicable.

**Informed Consent Statement:** Not applicable.

**Data Availability Statement:** Not applicable.

**Acknowledgments:** The authors also thank Borja Pena and Hiroto Kitamura (Former Undergraduate Students of Meiji University) for participating in the experiment.

**Conflicts of Interest:** The authors declare no conflict of interest.

## References

1. Meguro & Numada Lab of the University of Tokyo. Available online: <http://risk-mg.iis.u-tokyo.ac.jp/index.html> (accessed on 1 April 2023).
2. Holmes, M. Steel frames with brickwork and concrete infilling. *Proc. Inst. Civ. Eng.* **1961**, *19*, 473–478. [[CrossRef](#)]
3. Smith, S.B. Lateral stiffness of infilled frames. *J. Struct. Div.* **1962**, *88*, 183–199. [[CrossRef](#)]
4. Smith, S.B. Behaviour of the square infilled frames. *J. Struct. Div.* **1966**, *92*, 381–403. [[CrossRef](#)]
5. Smith, S.B.; Carter, C. A method of analysis for infill frames. *Proc. Inst. Civ. Eng.* **1969**, *44*, 31–48.
6. Mainstone, R.J. On the stiffness and strength of infilled frames. *Proc. Inst. Civ. Eng.* **1971**, *44*, 57–90.
7. Hendry, A.W. *Structural Masonry*; Macmillan: London, UK, 1998.
8. Applied Technology Council (ATC). *Evaluation of Earthquake Damaged Concrete and Masonry Wall Buildings*; FEMA 306: Redwood City, CA, USA, 1998.
9. Paulay, T.; Priestley, M.J.N. *Seismic Design of Reinforced Concrete and Masonry Buildings*; John Wiley & Sons, Inc: Hoboken, NJ, USA, 1992; pp. 584–592.
10. Shing, P.B.; Mehrabi, A.B. Behaviour and analysis of masonry-infilled frames. *Prog. Struct. Eng. Mater.* **2002**, *4*, 320–331. [[CrossRef](#)]
11. Cavaleri, L.; Trapani, F.D. Prediction of the additional shear action on frame members due to infills. *Bull. Earthq. Eng.* **2015**, *13*, 1425–1454. [[CrossRef](#)]
12. Jin, K.; Choi, H.; Nakano, Y. Experimental Study on Lateral Strength Evaluation of Unreinforced Masonry-Infilled RC Frame. *Earthq. Spectra* **2016**, *32*, 1725–1747. [[CrossRef](#)]
13. Mohammad, A.F.; Faggella, M.; Gigliotti, R.; Spacone, E. Seismic performance of older R/C frame structures accounting for infills-induced shear failure of columns. *Eng. Struct.* **2016**, *122*, 1–13. [[CrossRef](#)]
14. Suzuki, T.; Choi, H.; Sanada, Y.; Nakano, Y.; Matsukawa, K.; Paul, D.; Gulkan, P.; Binici, B. Experimental evaluation of the in-plane behaviour of masonry wall infilled RC frames. *Bull. Earthq. Eng.* **2017**, *15*, 4245–4267. [[CrossRef](#)]
15. Milanese, R.R.; Morandi, P.; Magenes, G. Local effects on RC frames induced by AAC masonry infills through FEM simulation of in-plane tests. *Bull. Earthq. Eng.* **2018**, *16*, 4053–4080. [[CrossRef](#)]
16. Alwashali, H.; Sen, D.; Jin, K.; Maeda, M. Experimental investigation of influences of several parameters on seismic capacity of masonry infilled reinforced concrete frame. *Eng. Struct.* **2019**, *189*, 11–24. [[CrossRef](#)]
17. Applied Technology Council (ATC). *Prestandard and Commentary for the Seismic Rehabilitation of Buildings*; FEMA 356: Reston, VA, USA, 2000.
18. American Society of Civil Engineers. *Seismic Rehabilitation of Existing Buildings*; ASCE Publications [ASCE/SEI 41-06]: New York, NY, USA, 2007.

19. Stavridis, A.; Shing, B. Simplified modeling of masonry-infilled RC frames subjected to seismic loads. In Proceedings of the 15th World Conference on Earthquake Engineering, Lisbon, Portugal, 24–28 September 2012.
20. Jin, K.; Choi, H. A simplified evaluation method of skeleton curve for RC frame with URM infill. *Earthq. Struct.* **2017**, *13*, 309–322.
21. Alwashali, H.; Torihata, Y.; Jin, K.; Maeda, M. Experimental observations on the inplane behaviour of masonry wall infilled RC frames; focusing on deformation limits and backbone curve. *Bull. Earthq. Eng.* **2018**, *16*, 1373–1397. [[CrossRef](#)]
22. Akhoundi, F.; Vasconcelos, G.; Lourenco, P.; Silva, L.C. Out-of-Plane Response of Masonry Infilled RC Frames: Effect of Workmanship and Opening. In Proceedings of the 16th International Brick and Block Masonry Conference, Padova, Italy, 26–30 June 2016.
23. Dizhur, D.; Walsh, K.; Giongo, I.; Derakhshan, H.; Ingham, J. Out-of-Plane Proof Testing of Masonry Infill Walls. *Structures* **2018**, *15*, 244–258. [[CrossRef](#)]
24. Petrone, C.; Magliulo, G.; Manfredi, G. Shake Table Tests for the Seismic Assessment of Hollow Brick Internal Partitions. *Eng. Struct.* **2014**, *72*, 203–214. [[CrossRef](#)]
25. Yu, J.H.; Park, J.H. Investigation of Steel Fiber-Reinforced Mortar Overlay for Strengthening Masonry Walls by Prism Tests. *Appl. Sci.* **2020**, *10*, 6395. [[CrossRef](#)]
26. Karalar, M.; Özkılıç, Y.O.; Aksoylu, C.; Sabri, M.M.; Beskopylny, A.N.; Stel'makh, S.A.; Shcherban, E.M. Flexural behavior of reinforced concrete beams using waste marble powder towards application of sustainable concrete. *Front. Mater.* **2022**, *9*, 1068791. [[CrossRef](#)]
27. Gilstrap, J.M.; Dolan, C.W. Out-of-plane bending of FRP-reinforced masonry walls. *Compos. Sci. Technol.* **1998**, *58*, 1277–1284. [[CrossRef](#)]
28. Sonia, M.; Elio, S. Modeling of reinforced masonry elements. *Int. J. Solids Struct.* **2001**, *38*, 4177–4198.
29. ElGawady, M.; Lestuzzi, P.; Badoux, M. A review of conventional seismic retrofitting techniques for URM. In Proceedings of the 13th International Brick and Block Masonry Conference, Amsterdam, The Netherlands, 4–7 July 2004.
30. Seki, M.; Popa, V.; Lozinca, E.; Dutu, A.; Papurcu, A. Experimental Study on Retrofit Technologies for Rc Frames with Infilled Brick Masonry Walls in Developing Countries. In Proceedings of the 16th European Conference on Earthquake Engineering, Thessaloniki, Greece, 18–21 June 2018.
31. Gattesco, N.; Boem, I. Out-of-Plane Behavior of Reinforced Masonry Walls: Experimental and Numerical Study. *Compos. Part B Eng.* **2017**, *128*, 39–52. [[CrossRef](#)]
32. Alwashali, H.; Sen, D.; Maeda, M.; Seki, M. Advantages and limitations of retrofitting masonry infilled RC Frames by Ferrocement based on experimental observations. In Proceedings of the 17th World Conference on Earthquake Engineering, Sendai, Japan, 26 September–2 October 2020.
33. Furtado, A.; Rodrigues, H.; Arêde, A.; Varum, H. Impact of the Textile Mesh on the Efficiency of TRM Strengthening Solutions to Improve the Infill Walls Out-of-Plane Behaviour. *Appl. Sci.* **2020**, *10*, 8745. [[CrossRef](#)]
34. Scamardo, M.; Cattaneo, S.; Biolzi, L.; Vafa, N. Parametric Analyses of the Response of Masonry Walls with Reinforced Plaster. *Appl. Sci.* **2022**, *12*, 5090. [[CrossRef](#)]
35. Priestley, M.J.N.; Bridgeman, D.O. Seismic Resistance of Brick Masonry Walls. *Bull. New Zealand Natl. Soc. Earthq. Eng.* **1974**, *7*, 167–187. [[CrossRef](#)]
36. Mayrhofer, C. Reinforced masonry walls under blast loading. *Int. J. Mech. Sci.* **2002**, *44*, 1067–1080. [[CrossRef](#)]
37. Haach, V.G.; Vasconcelos, G.; Lourenco, P.B. Study of the behaviour of reinforced masonry wallets subjected to diagonal compression through numerical modeling. In Proceedings of the 9th International Masonry Conference, Guimarães, Portugal, 7–9 July 2014.
38. Haile, F.; Corradi, M.; Adkins, J. Titanium rods with high mechanical properties were embedded into the horizontal mortar bed joint. In Proceedings of the Conservation of Architectural Heritage (CAH)—6th Edition, Sicily, Italy, 25–27 May 2022.
39. Triantafyllou, T.C.; Fardis, M.N. Strengthening of historic masonry structures with composite materials. *Mater. Struct.* **1997**, *30*, 486–496. [[CrossRef](#)]
40. Ma, R.; Jiang, L.; He, M.; Fang, C.; Liang, F. Experimental investigations on masonry structures using external prestressing techniques for improving seismic performance. *Eng. Struct.* **2012**, *42*, 297–307. [[CrossRef](#)]
41. Hwang, S.H.; Kim, S.; Yang, K.H. In-plane seismic performance of masonry wall retrofitted with prestressed steel-bar truss. *Earthq. Struct.* **2020**, *19*, 459–469.
42. Baqi, A.; Bhandari, N.M.; Trikha, D.N. Experimental study of prestressed masonry flexural elements. *J. Struct. Eng.* **1999**, *125*, 245–254. [[CrossRef](#)]
43. Phipps, M.E. Prestressed masonry. *Prog. Struct. Eng. Mater.* **2000**, *2*, 304–310. [[CrossRef](#)]
44. Foti, D.; Monaco, P. Post-tensioned masonry: State of the art. *Prog. Struct. Eng. Mater.* **2000**, *2*, 311–318. [[CrossRef](#)]
45. Wight, G.D.; Ingham, J.M.; Kowalsky, M.J. Shaketable testing of rectangular post-tensioned concrete masonry walls. *ACI Struct. J.* **2006**, *103*, 587.
46. Yang, K.H.; Mun, J.H.; Hwan, S.H. Cyclic shear behavior of masonry walls strengthened with prestressed steel bars and glass fiber grids. *Compos. Struct.* **2020**, *238*, 111961. [[CrossRef](#)]
47. ACI 530-02/ASCE 5-02/TMS 402-02; Building Code Requirements for Masonry Structures. Masonry Standards Joint Committee, 2002. Available online: <https://engineering.purdue.edu/~ramirez/CE479/FALL05/MasonryBuildingCode1-3-02.pdf> (accessed on 3 April 2023).

48. *TEK 14-20A*; Post-Tensioned Concrete Masonry Wall Design. National Concrete Masonry Association (NCMA): Herndon, VA, USA, 2001.
49. Jin, K.; Masuda, T.; Habara, Y.; Tomizawa, T. Structural Performance of Reinforced Masonry Member for Stilt House in Southeast Asia (Part 1: 3-Point Bending Test for unreinforced and reinforced masonry specimens). In *Summaries of Technical Papers of Annual Meeting*; Architectural Institute of Japan (AIJ): Hokkaido, Japan, 2022. (In Japanese)
50. Jin, K.; Song, S.; Kitayama, K.; Hao, L. Detailed evaluation of the ultimate flexural states of beams in unbonded precast prestressed concrete frames. *Bull. Earthq. Eng.* **2019**, *17*, 1495–1519. [[CrossRef](#)]
51. Jin, K.; Hao, L.; Kitayama, K. Direct evaluation method for load-deformation curve of precast prestressed concrete frame with different tendon forces. *Bull. Earthq. Eng.* **2021**, *19*, 3597–3626. [[CrossRef](#)]
52. Jin, K.; Ota, R.; Hao, L.; Kitayama, K. Evaluation Method for Ultimate Flexural State of Prestressed Precast Reinforced Concrete Beam–Column Connection with Debonded Partial Tendon. *Appl. Sci.* **2023**, *13*, 2843. [[CrossRef](#)]
53. Jin, K.; Kitayama, K.; Song, S.; Kanemoto, K. Shear Capacity of Precast Prestressed Concrete Beam–Column Joint Assembled by Unbonded Tendon. *ACI Struct. J.* **2017**, *114*, 51–62. [[CrossRef](#)]
54. Architectural Institute of Japan. *AIJ Standard for Structural Calculation of Reinforced Concrete Structures*; Architectural Institute of Japan (AIJ): Tokyo, Japan, 2018.

**Disclaimer/Publisher’s Note:** The statements, opinions and data contained in all publications are solely those of the individual author(s) and contributor(s) and not of MDPI and/or the editor(s). MDPI and/or the editor(s) disclaim responsibility for any injury to people or property resulting from any ideas, methods, instructions or products referred to in the content.